Microchemical Journal 209 (2025) 112663

Contents lists available at ScienceDirect

Microchemical Journal

journal homepage: www.elsevier.com/locate/microc

Detection of the doping agent formestane using a spectroscopic ellipsometric method with electrodeposited polydopamine-based molecular imprinting

Mustafa Oguzhan Caglayan [a,*], Zafer Üstündağ [b]

[a] Bilecik Seyh Edebali University, Bioengineering Department, Bilecik, Turkey
[b] Kütahya Dumlupınar University, Chemistry Department, Kutahya, Turkey

ARTICLE INFO

Keywords:
Designer steroids
Formestane
Molecular imprinting
Spectroscopic ellipsometry

ABSTRACT

Designer steroids are steroids produced in the laboratory by chemically modifying the steroid backbone to replace anabolic steroids. One of these steroids, formestane (4-hydroxyandrost-4-ene-3,17-dione, FMST), has been added to the list of substances prohibited in sports by the World Anti-Doping Agency (WADA) due to its positive effects in reducing the side effects of other doping steroids. A non-sophisticated yet relatively inexpensive method for detecting these steroids in adulterated dietary supplements is currently unavailable. In this study, for the first time, a spectroscopic ellipsometer (SE)-based sensor using polydopamine (pDA) as a molecularly imprinted polymer (MIP) recognition element was developed for the detection of FMST. FMST detection was achieved in the range of 10 pM–100 nM using MIP-pDA formed on a gold-coated silicon chip by the electropolymerization method. The detection limits (with a 3σ noise ratio) determined from the change in the ellipsometric angle Δ spectroscopically in the range of 600–700 nm and directly from the Δ value at a single wavelength were 310 and 382 pM, respectively. The sensor response on the non-imprinted polymer surface remained within noise limits. Recovery rates determined by spiking energy drinks and tablet-form vitamins were found to be greater than 95 %. In reusability tests, the signal obtained after 4 cycles was over 90 %. The usability of the developed MIP-pDA sensor for FMST detection was confirmed, and it was shown that it can be adapted to an SE method for the first time.

1. Introduction

The documented history of using various natural or synthetic chemicals for doping in sports competitions dates back many years [1]. The earliest recorded instances of doping are from the fifteenth century [2]. Reports have also documented the use of various alkaloids [3]. For anabolic steroid use in doping, injections of testosterone (17β-hydroxyandrost-4-en-3-one) and stanozolol ([1′,2′]-1′H-pyrazolo[4′,5′:2,3]-17α) have been noted [4]. Steroids are a class of chemical compounds consisting of three cyclohexane rings (**Fig. S1a**) and one cyclopentane ring. In steroids, there are various chemical structures with groups that can vary in many positions and different stereochemical forms [5]. An example of the structure of anabolic steroids is 17α-methyltestosterone (17β-hydroxy-17α-methylandrost-4-en-3-one) [6].

According to World Anti-Doping Agency (WADA) statistics, anabolic androgenic steroids (AAS) are involved in 48 % of doping cases [7]. Due to the long-lasting effects of anabolic steroids, out-of-competition doping screenings are a common practice, and WADA consistently bans steroid use among competing athletes. Since testosterone was first synthesized [8], extensive research has aimed to create steroid compounds with diverse and beneficial biological properties [9]. These syntheses have led to the introduction of new steroid derivatives with various modifications [6]. Laboratory-synthesized steroids, known as 'designer steroids,' are prevalent [10]. The first reported designer steroid in a doping case was norboletone (18β-homo-17β-hydroxy-19-nor-17α-preg-4-en-3-one) [10]. Despite bans and side effects, these steroids are readily available on the market for direct use or as a component of food/supplements [11]. The primary methods for detecting these substances are high-performance liquid chromatography (HPLC) and gas chromatography-mass spectrometry (GC–MS) [4,12]. However, these techniques often involve laborious sample preparation steps, including purification and chemical derivatization [4]. Consequently, ongoing

* Corresponding author.
E-mail address: mocaglayan@gmail.com (M.O. Caglayan).

https://doi.org/10.1016/j.microc.2025.112663
Received 4 July 2024; Received in revised form 16 December 2024; Accepted 2 January 2025
Available online 3 January 2025
0026-265X/© 2025 Elsevier B.V. All rights are reserved, including those for text and data mining, AI training, and similar technologies.

research focuses on developing alternative analytical methods for steroid detection.

Formestane (4-hydroxyandrosta-4,17-dione, FMST) is a pharmaceutical aromatase inhibitor that binds irreversibly and covalently to the active site of the P450 enzyme aromatase (**Fig. S1b**) [13]. It serves as a potential metabolite of androst-4-ene-3,17-dione, an intermediate in the biosynthesis of testosterone, and of 4,17β-dihydroxyandrosta-4-en-3-one [14]. In humans, estrogens strongly inhibit the pituitary release of gonadotropin-releasing factors. When estrogen synthesis is inhibited, luteinizing hormone (LH) levels increase. It has been reported that FMST intake results in a net increase in testosterone production [15]. Additionally, combining FMST with testosterone and/or its precursors (e.g., androstenedione) can mitigate aromatization-related side effects such as gynecomastia [16]. For these reasons, anti-estrogenic substances, including aromatase inhibitors, have been listed on WADA's Prohibited Substances List in Sports since 2004 [17]. Furthermore, the misuse and abuse of anabolic steroids cause adverse effects on all body tissues and organs. Anabolic steroids have been reported to lead to serious conditions such as hypogonadism, heart failure, neurodegeneration, coronary artery disease, and sudden cardiac death [18,19].

The primary analytical method for FMST is chromatography-based [13]. FMST can be endogenously produced in humans in trace amounts and detected in urine samples at low concentrations ranging from 0.5–20 ng/mL or as a result of pathological processes [20,21]. Since 2011, WADA regulations require an isotope ratio mass spectrometry (IRMS)-based verification to determine the synthetic origin of FMST before reporting a negative analytical finding for samples with concentrations below 150 ng/mL [17]. Detecting FMST at low concentrations should first be conducted using a more cost-effective and rapid method, followed by IRMS if necessary. Limited studies on FMST detection have been reported in the literature. Chromatographic methods such as gas chromatography (GC) coupled with tandem mass spectrometry (MS-MS) [22–24], GC combustion IRMS [25,26], ultra-high-performance liquid chromatography (UHPLC) with tandem MS [27,28], LC orbitrap MS [29], and LCMS [30] have been reported, with improvements in sample pre-processing. However, there are no studies on the detection of FMST using different recognition elements and sensor platforms. Studies examining the interaction between double-stranded DNA and FMST [31] and applying square-wave adsorptive anodic stripping voltammetry for its detection (detection limit, LOD, 7 nM) referencing anticancer drug applications [32], are available.

To address this gap in the literature, this study aims to develop an ellipsometric sensor for detecting FMST in aqueous solutions. Ellipsometry is an optical technique that measures changes in the polarization state of light reflected from thin films [33]. The sensitivity of this method largely depends on the ellipsometer's configuration. For instance, combining a spectrophotometric light source (e.g., a light source with a suitable monochromator ranging from 200 nm to 1200 nm) with an extremely precise goniometer (e.g., with a movement precision as low as 0.01°) provides very high sensitivity and accuracy regarding the dielectric functions of the examined surface. This configuration ensures good sensitivity for (bio)sensor applications. When SE is employed, the ellipsometric functions (i.e., delta (Δ) and psi (Ψ)) of an upper layer on the substrate where molecular interactions occur change significantly. The first function, Δ, is more sensitive to changes in the dielectric function of the substrate and shifts to lower degrees when molecular accumulation occurs due to the molecular recognition of the analyte by the recognition element. Considering Δ's sensitivity to molecular accumulation, this study aims to detect FMST using SE.

In this study, for the first time, molecularly imprinted polymers (MIPs) will be used for the detection of FMST using SE. MIPs are novel functional materials with molecular recognition capabilities specific to the target molecule [34]. These polymers are designed with a predetermined selectivity for any analyte, mimicking natural recognition elements such as antibodies and biological receptors. MIPs hold significant potential over traditional analytical methods and biosensors in the detection and/or monitoring of various analytes. Their key advantages, including ease of preparation, low cost, and extended shelf life, make them a preferred choice in many applications [35].

Electropolymerization serves as a robust method for forming uniform films on electrodes, offering a convenient means to adjust film thickness reproducibly by simply manipulating the number of deposition cycles [36]. In contrast to the conventional free radical polymerization, electropolymerization in MIPs occurs upon the oxidation of an appropriate functional monomer in the presence of a template. Dopamine (DA), an electropolymerizable monomer, interacts with various templates through non-covalent mechanisms like π-π stacking, electrostatic interactions, and hydrogen bonding [37]. DA has been innovatively used in molecular imprinting with electropolymerized polydopamine (pDA) films in a capacitive sensor for nicotine detection in human serum [38]. Combining ellipsometry with a pDA-based MIP, deemed advantageous for its selectivity and sensitivity, especially for FMST, has been considered appropriate. The SE platforms to be employed inherently utilize materials capable of reflection and aim for a smooth base material (maximum RMS < 2 nm). Typically, SE measurements are performed on Si wafers, however, in this study, Si wafers were coated with Au to facilitate the electropolymerization processes, and the MIP was deposited on this substrate via electropolymerization. This study aimed to develop a relatively simple, fast, and cost-effective analytical method for detecting steroids in adulterated food and dietary supplements by utilizing a highly sensitive ellipsometric technique combined with molecularly imprinted polymers as an advantageous recognition element. The schematic illustration of the method is depicted in Fig. 1.

2. Experimental

2.1. General

Chemicals and materials were acquired in analytical grade purity from local suppliers of Sigma-Aldrich and Merck and were used as received unless otherwise noted. Ultra-pure water (resistivity 18.2 MΩ cm, Millipore, USA) was employed for preparing all aqueous solutions. Phosphate-buffered saline (PBS) solution (0.01 M, pH 7.0) was used for preparing synthesis and analyte solutions, with pH adjustments made using HCl or NaOH, unless specified otherwise. Ellipsometric measurements were conducted using a spectrophotometric ellipsometer (Optosense, S6000, Turkey). The Si wafer was cleaned with an aggressive oxidizing treatment using a 4:1 (v/v) mixture of concentrated sulfuric acid and hydrogen peroxide, followed by a 30-minute cleaning with 100 W air plasma in a plasma device (Femtoscience, Korea), and then washed with ethanol/acetone. Unless stated otherwise, experimental studies utilized at least three replicates, and results were reported as mean ± standard deviation (σ).

2.2. Coating Si Wafers with Au Film

To facilitate dopamine electropolymerization, Si wafers were coated with a 10 nm layer of Au. The wafers underwent aggressive oxidant treatment using a 4:1 (v/v) solution of concentrated sulfuric acid and hydrogen peroxide, followed by a 30-minute cleaning with 100 W air plasma in a plasma device (Femtoscience, Korea), and were finally washed with ethanol/acetone. Metal coating was applied to the substrate through physical vapor deposition (PVD, Nanovak, Turkey), which included an adhesive layer (3 nm Cr) beneath the 10 nm Au layer. The prepared chips were then cleaned with plasma for 20 min prior to the MIP coating procedures.

2.3. Formation and Characterization of Dopamine MIP and Non-Imprinted Films

pDA-coated electrodes were prepared and characterized as outlined in the literature [36]. The electrochemical characterization of pDA

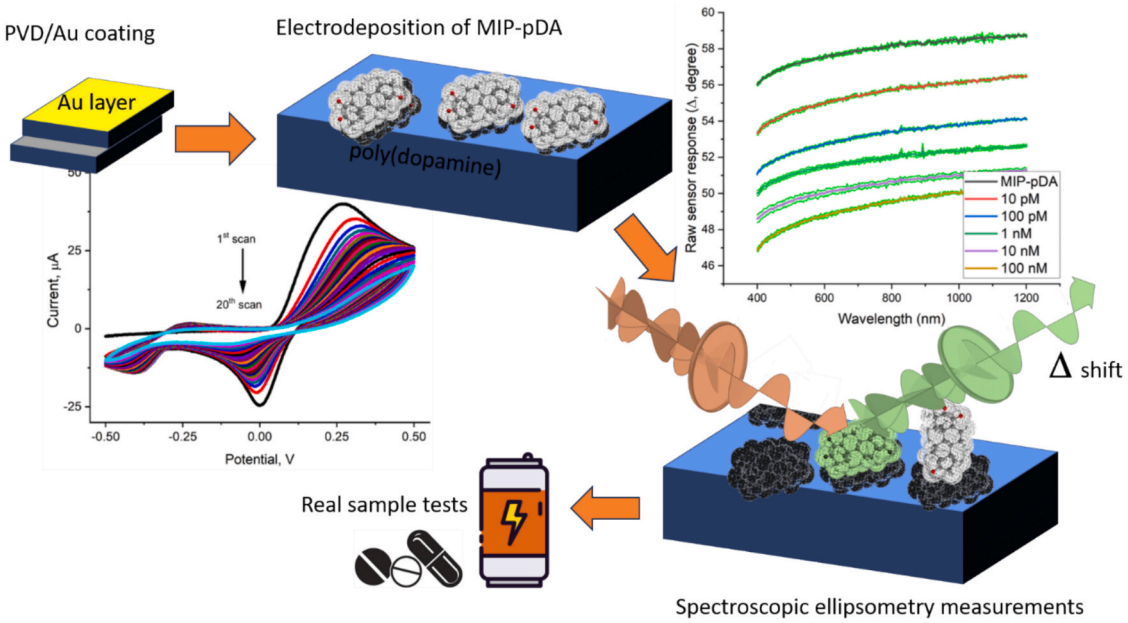

Fig. 1. A schematic overview of the experimental procedure: coating the Si-wafer for DA electropolymerization, creating MIP-pDA with the template (FMST), analyzing the interaction between MIP-pDA and FMST using spectroscopic ellipsometry, and evaluating the sensor platform in energy drinks and dietary supplements.

surfaces utilized an Au disc electrode (BASi, MF-2014, USA) with a 1.6 mm diameter. This electrode was connected as the working electrode in a low-volume electrochemical cell (BASi) within a standard three-electrode setup. A 1 mg/mL DA solution was prepared by dissolving DA-HCl in a 10 mM phosphate buffer at pH 7.4, saturated with nitrogen. For MIP-pDA films, the required amount of FMST was added according to the desired DA/FMST ratio (20:1, 10:1, or 5:1 M ratio). The solution was then transferred to the reactor and purged with nitrogen before undergoing polymerization via cyclic voltammetry (CV) from −0.5 V to + 0.5 V at a scan rate of 0.2 V/s for 1–20 cycles. The electrode was subsequently removed and washed sequentially with deionized water, a methanol ammonia solution (pH 9) (1:1, v/v), methanol, and again with deionized water. Reference non-imprinted pDA films (NIP-pDA) were synthesized similarly but without the template removal step. The insulating pDA layer on the gold electrodes was characterized using 2 mM potassium ferricyanide, $K_3[Fe(CN)_6]$, in 10 mM phosphate buffer at pH 7.4 [39,40].

For ellipsometric platforms, the electrochemical polymerization to form MIP on the Au-coated Si wafer surface was conducted as previously described [36]. The Au-coated Si wafer pieces (electrodes) were first cleaned with piranha solution (H_2SO_4/H_2O_2 4:1, v/v) for 1 min, thoroughly rinsed with deionized water, and dried under nitrogen. Then, a 1 mg/mL dopamine (DA) solution and FMST at DA/FMST ratios of 20:1, 10:1, and 5:1 (pH 7.4, PBS) were saturated with nitrogen and subjected to 20 cycles of CV to imprint FMST into pDA. The non-imprinted polymer (NIP) was prepared similarly but without the template molecule.

2.4. AFM images, ellipsometric thickness measurements, and FTIR analyses

The thickness and dielectric constant of the pDA layer on each sensor chip were measured using an ellipsometer, considering both Δ and Ψ values, and the built-in software of the device. Measurements were taken at 10 randomly selected points on 3 different test samples, with results reported as the average value (±1σ). AFM topography images of the NIP-pDA, MIP-pDA, and FMST-MIP-pDA surfaces were captured in non-contact mode over a 2 μm x 2 μm area using a ParkSystems XE-100 AFM (Korea). From these images, root mean square (RMS) roughness (Rq) values were calculated and compared by selecting two 1x1 μm areas from the same image and a total of 10 areas from 5 different surfaces. Additionally, ATR-FTIR (Attenuated Total Reflection-Fourier Transform Infrared Spectroscopy, Bruker-Alpha) data for NIP-pDA and FMST-MIP-pDA surfaces were collected in the range of 400–4000 cm^{-1} and compared.

2.5. Detection of FMST and evaluation of analytical performance using spectroscopic ellipsometry measurements

The analytical performance of the MIP platform in detecting FMST was assessed using FMST solutions in ethanolic PBS buffer (pH 7.4), with concentrations ranging from 10 pM to 100 nM. The Au-coated Si wafers carrying the MIP platform were exposed to FMST solutions for 30 min, then washed with buffer solution. The dried wafers were analyzed using a spectroscopic ellipsometer (SE) at a 60° angle of incidence with monochromatic and polarized light ranging from 400 to 1200 nm. Ellipsometric parameters, delta (Δ) and psi (Ψ), were measured. The Δ angle, representing the phase shift between polarized and reflected light, was used as the sensor response due to its higher sensitivity to surface accumulation. Molecular accumulation on the surface alters its thickness and dielectric properties. The Δ spectrum around the wavelength range of 600–690 nm showed a nearly linear Δ-λ relationship. The results from spectroscopic ellipsometry were reported as six analyses from three different samples, with two measurements taken from each chip to verify uniformity (N = 6). Standard deviation (σ) was shown as a band on the graphs to indicate uncertainty limits. It was noted that Δ shifted towards lower values with surface accumulation. Thus, two different sensor calibration graphs were created using both the Δ value at the intercept (±σ) and the single Δ value (±σ) at the median wavelength. LOD values were derived from the calibration graph based on a 3σ noise ratio exceeding a 95 % confidence interval [41]. Binding isotherms were generated using values determined at each analyte concentration, and coefficients for each isotherm were obtained by fitting the data to Langmuir and Freundlich adsorption models [42].

2.6. Selectivity, reusability, and real sample tests

Standard addition methods were employed for selectivity and real sample tests. Steroid-free sports drinks and dietary supplement tablets

from a local market were chosen to simulate real sample testing conditions. The sports drink, according to its label, contains caffeine, niacin, taurine, vitamins, acidity regulators, and sugars. These drinks were filtered through a 0.45-μm syringe filter and analyzed without further processing (Zielińska et al. 2022).

FMST was added to the ground tablets and directly to the sports drink to achieve the desired final concentration. The samples were then subjected to methanol extraction (Van Poucke et al. 2007). After coarse filtration of solid components and subsequent filtration through a 0.45-μm syringe filter, measurements were conducted. In the selectivity experiments, other steroids such as 11-aldosterone (ASTRN) and cholesterol (CHOL) were used. Analytical performance was assessed by measuring recovery values through separate and simultaneous additions at high, middle, and low concentration ranges within the measurement range. To evaluate the reusability of FMST-MIP-pDA, analyses were performed after adding 5 nM and 50 nM FMST to the sports drink sample, followed by regeneration using a washing solution (acetic acid: methanol (HAc: MetOH); 1:9, 60 °C).

3. Results and discussion

3.1. Formation and characterization of dopamine MIP and non-imprinted (NIP) films

The cyclic voltammograms of 1 mg/mL DA in 10 mM phosphate buffer at pH 7.4 (scan rate 0.2 V/s, vs. Ag/AgCl/KCl_{sat}) is shown in **Fig. S2**. It is evident that DA begins to polymerize and modify the Au surface due to oxidation from the first scan (**FigureS3**). The conductivity of the Au surface towards DA decreases with each scan, indicating that the Au surface is being coated with pDA. The peak current, initially around 23.1 μA in the first scan, decreases to 14.4 μA by the 5th scan, representing a reduction of approximately 40 %. By the final scan, the peak current has decreased to a negligible level. Based on these cycles, the electrochemical characterization of the bare Au and the modified electrode surfaces after the 5th and 20th scans was conducted using 2 mM $K_3[Fe(CN)_6]$ (in 10 mM phosphate buffer at pH 7.4) as a redox probe (**Fig. S4**). On the bare Au surface, the electron transfer of the redox probe is very rapid (anodic peak current 30.8 μA), whereas in the 5th scan, the electron transfer significantly slows down (anodic peak current 6.6 μA). After the twentieth scan, the electron transfer of the redox probe on the electrode surface is completely blocked. This confirms the polymerization of DA on the Au surface.

To optimize the DA ratio in MIP production, MIPs with monomer/FMST ratios of 5:1, 10:1, and 20:1 were used to detect 2 μM FMST, resulting in Δ values of 40.03 ± 0.09°, 43.01 ± 0.11°, and 45.02 ± 0.10°, respectively. Given the shift of Δ to lower values with the accumulation of FMST on the MIP surface, it was observed that a lower monomer ratio, despite not showing a significant difference, led to a higher sensor response. Consequently, MIP-pDA surfaces were prepared at a 5:1 DA/FMST ratio. This ratio aligns with target/monomer ratios reported in the literature [43].

3.2. AFM images, ellipsometric thickness measurements, and FTIR analyses

The characterization of samples obtained after 20 cycles of electropolymerization (NIP-pDA) and samples imprinted with FMST (FMST-MIP-pDA) was conducted using ellipsometric thickness measurements, AFM images, and FTIR analyses. During the electropolymerization stage, the thickness of the accumulated pDA layer on the sensor chip surface and dielectric constant measurements were determined using both Δ and Ψ values with the ellipsometer and the built-in software of the equipment, utilizing library data for Si/Cr/Au/polymer layers (**Fig. S5**). Ellipsometric thickness for NIP-pDA indicates the thickness of pDA accumulated through electrochemical deposition after 20 cycles. For FMST-saturated MIP-pDA, the thickness was slightly higher compared to NIP-pDA. This could be attributed to FMST filling the voids in the pDA structure, which were not accounted for in the modeling, rather than contributing to the thickness. However, MIP-pDA yielded slightly higher thickness values compared to FMST-MIP-pDA surfaces treated with regeneration solution, indicating partial completion of regeneration for the saturated surface. Nonetheless, it should be noted that the more uniform thickness observed in NIP-pDA is not observed in MIP-pDA.

AFM topography images were captured over a 2 μm x 2 μm area in non-contact mode. These images reveal plate-like formations characteristic of pDA and display small porous structures, aligning with pDA morphology as reported in the literature [44]. In **Fig. S6**, there appears to be no significant distinction observed in the topographic images of NIP-pDA, FMST-saturated MIP-pDA, and the surface regenerated from the saturated film of blank MIP-pDA.

Ten RMS roughness, Rq, values were determined from these images, comprising two areas of 2x1 μm each within the same image and from five different surfaces (**Fig. S7**). It was observed that the roughness of the NIP-pDA surface is notably lower compared to both the FMST-saturated MIP-pDA and the MIP-pDA surfaces treated with regeneration solution. This suggests the concentration of FMST sites on the surface and confirms the occurrence of FMST detection at these sites.

Moreover, data from ATR-FTIR were obtained for both NIP-pDA and FMST-MIP-pDA surfaces and compared across the range of 400–4000 cm^{-1} (**Fig. S8**). The spectrum representing pure FMST exhibits primary and secondary peaks typical of FMST. In the spectrum attributed to pDA, peaks observed at 1510 and 1333 cm^{-1} correspond to C = N and C–N–C stretching vibrations, respectively [45]. While the distinction between peaks in the FMST spectrum and those in the pDA spectrum may not be pronounced due to the low FMST concentration, notably, peaks around 1730 cm^{-1} indicating C = O stretching, 1670 cm^{-1} indicating C = O aromatic stretching, 1630 cm^{-1} indicating C-O stretching, 2950 cm^{-1} indicating overtones, and 3380 cm^{-1} indicating OH stretching in the FMST-MIP-pDA spectrum, confirm the presence of FMST within the FMST-MIP-pDA structure.

3.3. Detection of FMST and assessment of analytical performance through spectroscopic ellipsometry measurements

The interaction between NIP-pDA and FMST was investigated, revealing that the sensor response for 2 μM FMST showed only a 0.98 ± 0.4 % increase in Δ values compared to NIP-pDA. This finding aligns broadly with existing literature and suggests a recognition mechanism predominantly mediated by template regions rather than nonspecific adsorption. The analytical performance of the MIP platform in FMST detection was assessed using an ethanol buffer solution containing FMST concentrations ranging from 10 pM to 100 nM. The unprocessed spectroscopic ellipsometry data (Δ-λ) are depicted in Fig. 2. It's evident that the Δ value for MIP-pDA (blank), spanning the 400–1200 nm range, initially stood at approximately 55-57° but gradually shifted towards lower Δ values with escalating FMST concentrations, consistently following the same pattern without accumulating phase shift alterations. Notably, the standard deviation values, depicted as a band around the average change on the graph, appear to be independent of both concentration and wavelength. This deviation is indicative of random errors rather than systematic ones.

The Δ spectrum obtained in the range of 600–690 nm displayed a linear Δ-λ relationship (**Fig. S9**). The intersection points from this linear region, along with their respective standard error values, were detailed in **Table S1**. Calibration curves were then constructed based on these intersection points (Fig. 3), utilizing the intersection point error as the σ value to determine the LOD. Additionally, an effort was made to establish the calibration curve using solely the Δ value obtained at a single wavelength, without spectral scanning. To this end, a statistical evaluation of the Δ-λ relationship in the linear region was performed. As shown in **Table S2**, the device collected a total of 35 Δ values for 35 wavelengths (λ). The median of these values corresponded

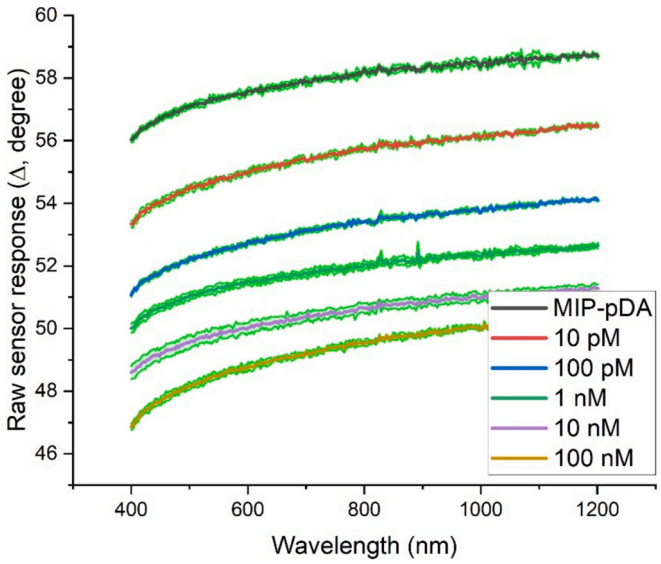

Fig. 2. Raw sensor response obtained with the addition of FMST (Δ-λ relationship).

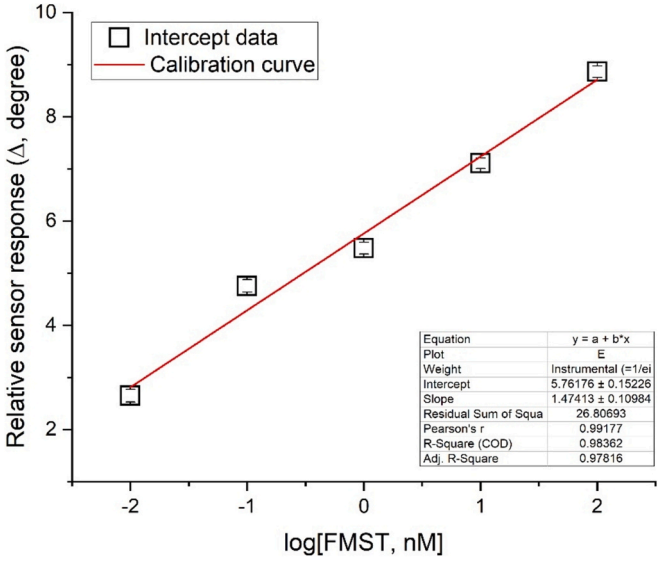

Fig. 3. Calibration curve obtained from the intersection point of the linear relationship between Δ and λ in the 600–690 nm range, along with statistical evaluations of the curve (inset).

approximately to a wavelength range of 650–655 nm. Utilizing the median values, a calibration curve was generated and presented in **Fig. S10**.

The calibration curve, derived from the linear region of the Δ-λ relationship between 600–690 nm, exhibited a highly consistent linear change when plotted in a log-linear format (against log[FMST]), displaying a determination coefficient (COD) of 0.98. This suggests a strong adherence to linearity. The results were normalized using the sensor response obtained from MIP-pDA and adjusted from a negative to a positive correlation. Additionally, employing median values for the calibration curve resulted in a slightly lower COD, though it remained relatively similar. This emphasizes the potential for SE analyses to reliably detect FMST with measurements within the 650–655 nm range. Nevertheless, considering potential inconsistencies in chip fabrication, spectral analysis was conducted across the entire spectrum, and data from the linear Δ-λ relationship in the 600–690 nm range were utilized to derive both the intersection point and the calibration curve. The analytical parameters obtained from the calibration curves are presented in Table 1.

To ascertain the sensor's maximum available FMST sites and unravel the FMST binding mechanism, SE measurements were conducted with FMST concentrations up to 2.5 μM. At a concentration of 2.0 μM FMST, a Δ change of 40.12 ± 0.08° was recorded. Taking this value as 100 % surface loading, the sensor's adherence to the Langmuir isotherm, expressed as $y = (y_m K[FMST])/(1 + K[FMST])$, was found to be notably low (with a COD of 0.832). The y_m and K coefficients for the isotherm were determined to be 0.486 ± 0.081 and 55.049 ± 3.145, respectively. Conversely, the adherence of the same parameters to the Freundlich isotherm, expressed as $y = \left(K[FMST]^{1/n}\right)$, yielded a higher COD ($R^2$, 0.968). The K and n coefficients were found to be 0.356 ± 0.018 and 7.734 ± 0.703, respectively. Favoring the Freundlich isotherm implies the heterogeneous nature of FMST adsorption sites on the MIP, with no indication of a multi-layer adsorption tendency within the studied concentration range. However, literature suggests that adsorption on the MIP can be better described by the Freundlich isotherm [46,47].

3.4. Selectivity, reusability, and real sample tests

In selectivity experiments, ethanol solutions of ASTRN and CHOL at concentrations of 5, 10, and 100 nM were used. Each analyte was individually, in combination with FMST, and all together interacted with the sensor, and the resulting sensor signals were compared (Fig. 4). As observed, CHOL produced results close to the noise signal in all added concentrations. However, ASTRN resulted in a signal that increased with increasing concentration but remained below the 3σ noise level. Structurally similar to FMSTN, the interference effect of this analyte was also examined at higher concentrations, and it was observed that ASTRN triggered a relative Δ value increase from 4.7 to 5.1 when stimulated at the FMST saturation concentration (2.0 μM), but this value still remained at the LOD threshold.

The detection results of 5, 50, and 100 nM FMST added to energy drinks (N1-N3) and dietary supplement tablets (N4-N6) are presented in Fig. 5. Across all sample measurements (N = 108), a positive bias was obtained. The maximum recovery was 126 %, while the minimum recovery was 88.3 %. The average recoveries in all addition experiments were 107.4 % ± 2.9 %, with no significant difference observed between sports drinks and dietary supplement tablets.

In the sensor's reusability study, we performed analyses for 5 nM and 50 nM FMST added to sample N1. The reusability data, obtained by regenerating with a washing solution after FMST injection, are depicted in **Fig. S11**. It demonstrates a swift decline in accuracy at low concentrations post-regeneration. However, for higher concentrations, it's noted that even after six regenerations, there's still satisfactory analytical accuracy. Yet, achieving a 90 % recovery after the fourth regeneration for 5 nM FMST suggests that the sensor platform developed can be regenerated and reused for actual sample applications up to three times.

4. Conclusion

In this research, we proposed an alternative detection platform for FMST (4-hydroxyandrost-4-ene-3,17-dione), a designer steroid previously undetectable by any sensor platform. FMST poses health risks

Table 1
Analytical parameters obtained from the calibration curves.

	Equation	3σ (Δ)	LOD (3σ/Slope)
From intercept of 600–690 nm line	$1.474(\log[FMST]) + 5.762$	0.457	0.310 nM
From median	$1.489(\log[FMST]) + 5.921$	0.569	0.382 nM

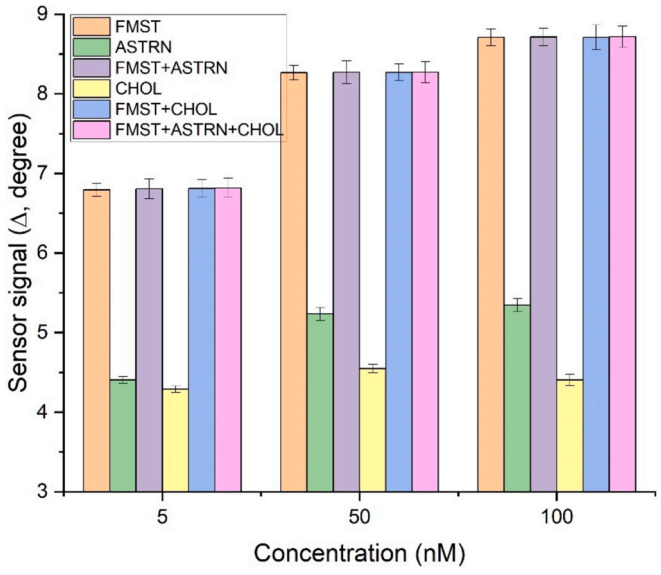

Fig. 4. Interference experiment results with ASTRN and CHOL.

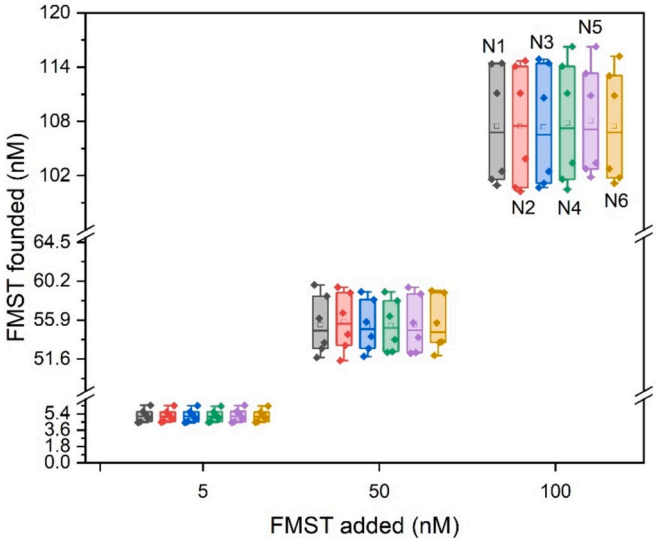

Fig. 5. FMST recoveries in three different brands of energy drinks (N1-N3) and three different dietary supplement tablets (N4-N6).

similar to other anabolic steroids, contributing to cardiovascular diseases and being illicit for doping purposes. Detecting FMST in various samples, such as adulterated products, typically demands complex and costly methods due to its hydrophobic nature and low molecular weight, presenting a challenge for different sensor platforms. Therefore, we favored ellipsometry as a sensitive transducer and molecularly imprinted polymer as a recognition element. FMST detection was successfully accomplished using MIP-pDA deposited on Au-coated Si chips via electropolymerization, within a range of 10 pM to 100 nM, with a detection limit as low as 310 pM. The new FMST detection technique presented in this article has demonstrated an analytical performance comparable to the limited number of studies in the literature. For example, in a voltammetric sensor study, a range of 0.19–2.91 μM with a detection limit of 62 nM for FMST was achieved [48]. In another electrochemical sensor study, a working range of 0.02–5.2 μM with a detection limit of 7.14 nM was reported [32].

While the MIP-based sensor showed a slight increase in response to two interfering agents, ASTRN and CHOL, it remained below the noise level. The average recovery rate of FMST spiked into energy drinks and dietary supplement tablets was 107 %, with a maximum recovery of 126 % and a minimum recovery of 88.3 %. In reuse tests, the signal obtained after 3 cycles exceeded 90 %. Consequently, the objective of developing an SE-based sensor using pDA as the MIP recognition element was effectively accomplished.

CRediT authorship contribution statement

Mustafa Oguzhan Caglayan: Writing – original draft, Supervision, Project administration, Funding acquisition, Data curation. **Zafer Üstündağ:** Investigation, Methodology, Writing – original draft, Validation.

Declaration of competing interest

The authors declare that they have no known competing financial interests or personal relationships that could have appeared to influence the work reported in this paper.

Acknowledgments

This study was financially supported by the Scientific Research Projects Coordination Department of Bilecik Seyh Edebali University under project number 2023-01.BŞEÜ.03-03.

Appendix A. Supplementary data

Supplementary data to this article can be found online at https://doi.org/10.1016/j.microc.2025.112663.

Data availability

No data was used for the research described in the article.

References

[1] H. Thompson, Superhuman athletes, Nature 487 (2012) 287.
[2] A. Higgins, PL04 From ancient Greece to modern Athens: 3000 years of doping in competition horses, J. Vet. Pharmacol. Ther. 29 (2006) 4–8.
[3] D.M. Rosen, Dope: a history of performance enhancement in sports from the nineteenth century to today, ABC-CLIO, 2008.
[4] A.R. McKinney, Modern techniques for the determination of anabolic–androgenic steroid doping in the horse, Bioanalysis 1 (2009) 785–803.
[5] G. Moss, Nomenclature of steroids (Recommendations 1989), Pure Appl. Chem. 61 (1989) 1783–1822.
[6] C.C. Waller, M.D. McLeod, A review of designer anabolic steroids in equine sports, Drug Test. Anal. 9 (2017) 1304–1319.
[7] I. Athanasiadou, S. Voss, E. Lyris, A. Aljaber, M. Alsayrafi, C. Georgakopoulos, Analytical progresses of the World Anti-Doping Agency Olympic laboratories: a 2016 update from London to Rio, Bioanalysis, 8 (2016) 2265-2279.
[8] R. Clinton, A. Manson, F. Stonner, H. Neumann, R. Christiansen, R. Clarke, J. Ackerman, D. Page, J. Dean, W. Dickinson, Steroidal [3, 2-c] pyrazoles. II. 1 Androstanes, 19-norandrostanes and their unsaturated analogs, Journal of the American Chemical Society, 83 (1961) 1478-1491.
[9] D.H. Catlin, B.D. Ahrens, Y. Kucherova, Detection of norbolethone, an anabolic steroid never marketed, in athletes' urine, Rapid Commun. Mass Spectrom. 16 (2002) 1273–1275.
[10] G. Buzby Jr, C. Walk, H. Smith, Totally synthetic steroid hormones. X. 1 Some (±)-13β-Ethyl-7α-methylgonane derivatives, J. Med. Chem. 9 (1966) 782–784.
[11] M.K. Parr, M. Gütschow, J. Daniels, G. Opfermann, M. Thevis, W. Schänzer, Identification of steroid isoxazole isomers marketed as designer supplement, Steroids 74 (2009) 322–328.
[12] J.P. Scarth, P. Teale, T. Kuuranne, Drug metabolism in the horse: a review, Drug Test. Anal. 3 (2011) 19–53.
[13] G.N. Leung, W. Kwok, T.S. Wan, K.K. Lam, P.J. Schiff, Metabolic studies of formestane in horses, Drug Test. Anal. 5 (2013) 412–419.
[14] J. Scarth, C. Akre, L. Van Ginkel, B. Le Bizec, H. De Brabander, W. Korth, J. Points, P. Teale, J. Kay, Presence and metabolism of endogenous androgenic–anabolic steroid hormones in meat-producing animals: a review, Food Addit. Contam. 26 (2009) 640–671.
[15] G.J. van Londen, S. Perera, K. Vujevich, P. Rastogi, B. Lembersky, A. Brufsky, V. Vogel, S.L. Greenspan, The impact of an aromatase inhibitor on body composition and gonadal hormone levels in women with breast cancer, Breast Cancer Res. Treat. 125 (2011) 441–446.

[16] D.S. Willoughby, C. Wilborn, L. Taylor, W. Campbell, Eight weeks of aromatase inhibition using the nutritional supplement Novedex XT: effects in young, eugonadal men, Int J Sport Nutr Exerc. Metab. 17 (2007) 92–108.
[17] X. de la Torre, D.M. Brito, C. Colamonici, M. Parr, F. Botre, Metabolism of formestane in humans: Identification of urinary biomarkers for antidoping analysis, Steroids 146 (2019) 34–42.
[18] G. Kanayama, H.G. Pope, J.I. Hudson, Associations of anabolic-androgenic steroid use with other behavioral disorders: an analysis using directed acyclic graphs, Psychol. Med. 48 (2018) 2601–2608.
[19] G.D. Albano, F. Amico, G. Cocimano, A. Liberto, F. Maglietta, M. Esposito, G.L. Rosi, N. Di Nunno, M. Salerno, A. Montana, Adverse effects of anabolic-androgenic steroids: A literature review, Healthcare, MDPI, 2021, pp. 97.
[20] T. Piper, G. Fusshöller, C. Emery, W. Schänzer, M. Saugy, Investigations on carbon isotope ratios and concentrations of urinary formestane, Drug Test. Anal. 4 (2012) 942–950.
[21] G. Poon, M. Jarman, R. McCague, J. Davies, C. Heeremans, R. Van der Hoeven, W. Niessen, J. Van der Greef, Identification of 4-hydroxyandrost-4-ene-3, 17-dione metabolites in prostatic cancer patients by liquid chromatography—mass spectrometry, J. Chromatogr. B Biomed. Sci. Appl. 576 (1992) 235–244.
[22] Y. Zhang, X. Wu, W. Wang, J. Huo, J. Luo, Y. Xu, J. Lu, Simultaneous detection of 93 anabolic androgenic steroids in dietary supplements using gas chromatography tandem mass spectrometry, J. Pharm. Biomed. Anal. 211 (2022).
[23] A.S. Kollmeier, X. de la Torre, C. Müller, F. Botrè, M.K. Parr, In-depth gas chromatography/tandem mass spectrometry fragmentation analysis of formestane and evaluation of mass spectral discrimination of isomeric 3-keto-4-ene hydroxy steroids, Rapid Commun. Mass Spectrom. 34 (2020).
[24] A.S.Y. Wong, G.N.W. Leung, D.K.K. Leung, T.S.M. Wan, Doping control analysis of anabolic steroids in equine urine by gas chromatography-tandem mass spectrometry, Drug Test. Anal. 9 (2017) 1320–1327.
[25] L. Honesova, P. Van Eenoo, M. Polet, A uniform sample preparation procedure for gas chromatography combustion isotope ratio mass spectrometry for all human doping control relevant anabolic steroids using online 2/3-dimensional liquid chromatography fraction collection, Anal. Chim. Acta 1168 (2021).
[26] M. Polet, P. Van Renterghem, W. Van Gansbeke, P. Van Eenoo, Profiling of urinary formestane and confirmation by isotope ratio mass spectrometry, Steroids 78 (2013) 1103–1109.
[27] F. Gosetti, E. Mazzucco, M.C. Gennaro, E. Marengo, Ultra high performance liquid chromatography tandem mass spectrometry determination and profiling of prohibited steroids in human biological matrices. A Review, J. Chromatogr. B: Anal. Technol. Biomed. Life Sci. 927 (2013) 22–36.
[28] S. Liu, G.G. Ying, J.L. Zhao, F. Chen, B. Yang, L.J. Zhou, H.J. Lai, Trace analysis of 28 steroids in surface water, wastewater and sludge samples by rapid resolution liquid chromatography-electrospray ionization tandem mass spectrometry, J. Chromatogr. A 1218 (2011) 1367–1378.
[29] E.D. Virus, T.G. Sobolevsky, G.M. Rodchenkov, Introduction of HPLC/orbitrap mass spectrometry as screening method for doping control, J. Mass Spectrom. 43 (2008) 949–957.
[30] M. Mazzarino, F. Botrè, A fast liquid chromatographic/mass spectrometric screening method for the simultaneous detection of synthetic glucocorticoids, some stimulants, anti-oestrogen drugs and synthetic anabolic steroids, Rapid Commun. Mass Spectrom. 20 (2006) 3465–3476.
[31] Y. Temerk, M. Ibrahim, H. Ibrahim, M. Kotb, Interactions of an anticancer drug Formestane with single and double stranded DNA at physiological conditions, J. Photochem. Photobiol. B Biol. 149 (2015) 27–36.
[32] H.M. Ali, I.A. Alhagri, H. Ibrahim, Fabrication of an electrochemical sensor based on gold nanoparticle-functionalized nanocarbon black hybrid nanocomposite for sensitive detection of anti-cancer drug formestane in biological and pharmaceutical samples, J. Electroanal. Chem. 907 (2022).
[33] M. Poksinski, H. Arwin, Protein monolayers monitored by internal reflection ellipsometry, Thin Solid Films 455 (2004) 716–721.
[34] L. Chen, X. Wang, W. Lu, X. Wu, J. Li, Molecular imprinting: perspectives and applications, Chem. Soc. Rev. 45 (2016) 2137–2211.
[35] A.G. Ayankojo, J. Reut, R. Boroznjak, A. Öpik, V. Syritski, Molecularly imprinted poly (meta-phenylenediamine) based QCM sensor for detecting Amoxicillin, Sens. Actuators B 258 (2018) 766–774.
[36] B. Stöckle, D.Y.W. Ng, C. Meier, T. Paust, F. Bischoff, T. Diemant, R.J. Behm, K. E. Gottschalk, U. Ziener, T. Weil, Precise control of polydopamine film formation by electropolymerization, Macromolecular Symposia, Wiley Online, Library (2014) 73–81.
[37] D.R. Dreyer, D.J. Miller, B.D. Freeman, D.R. Paul, C.W. Bielawski, Perspectives on poly (dopamine), Chem. Sci. 4 (2013) 3796–3802.
[38] K. Liu, W.-Z. Wei, J.-X. Zeng, X.-Y. Liu, Y.-P. Gao, Application of a novel electrosynthesized polydopamine-imprinted film to the capacitive sensing of nicotine, Anal. Bioanal. Chem. 385 (2006) 724–729.
[39] D. Işık, S. Şahin, M.O. Caglayan, Z. Üstündağ, Electrochemical impedimetric detection of kanamycin using molecular imprinting for food safety, Microchem. J. 160 (2021) 105713.
[40] N.M. Ali, M. Roushani, Z.M. Karazan, Novel Electrochemical Sensor Based on Polydopamine Molecularly Imprinted Polymer for Selective Determination of Methylergonovine Maleate, IEEE Sens. J. 24 (2024) 1140–1146.
[41] I.A. Kariper, Z. Üstündağ, M.O. Caglayan, A sensitive spectrophotometric ellipsometry based Aptasensor for the vascular endothelial growth factor detection, Talanta 225 (2021) 121982.
[42] K. Zhi, L. Wang, Y. Zhang, Y. Jiang, L. Zhang, A. Yasin, Influence of Size and Shape of Silica Supports on the Sol-Gel Surface Molecularly Imprinted Polymers for Selective Adsorption of Gossypol, Materials (Basel, Switzerland) 11 (2018).
[43] K.F. Pratama, M.E.R. Manik, D. Rahayu, A.N. Hasanah, Effect of the Molecularly Imprinted Polymer Component Ratio on Analytical Performance, Chem. Pharm. Bull. 68 (2020) 1013–1024.
[44] J. Lin, S. Daboss, D. Blaimer, C. Kranz, Micro-Structured Polydopamine Films via Pulsed Electrochemical Deposition, Nanomaterials 9 (2019) 242.
[45] C.-W. Hsu, M.-C. Yang, Enhancement of the imprinting effect in cholesterol-imprinted microporous silica, J. Non Cryst. Solids 354 (2008) 4037–4042.
[46] C.-M. Dai, J. Zhang, Y.-L. Zhang, X.-F. Zhou, Y.-P. Duan, S.-G. Liu, Removal of carbamazepine and clofibric acid from water using double templates–molecularly imprinted polymers, Environ. Sci. Pollut. Res. 20 (2013) 5492–5501.
[47] G.T. Rushton, C.L. Karns, K.D. Shimizu, A critical examination of the use of the Freundlich isotherm in characterizing molecularly imprinted polymers (MIPs), Anal. Chim. Acta 528 (2005) 107–113.
[48] M. Ibrahim, Y. Temerk, H. Ibrahim, M. Kotb, Indium oxide nanoparticles modified carbon paste electrode for sensitive voltammetric determination of aromatase inhibitor formestane, Sens. Actuators B 209 (2015) 630–638.